J|A|C|S
ARTICLES
Published on Web 03/19/2005

Potentiometric, Electronic Structural, and Ground- and Excited-State Optical Properties of Conjugated Bis[(Porphinato)zinc(II)] Compounds Featuring Proquinoidal Spacer Units

Kimihiro Susumu, Timothy V. Duncan, and Michael J. Therien*

Contribution from the Department of Chemistry, University of Pennsylvania, Philadelphia, Pennsylvania 19104-6323

Received October 28, 2004; E-mail: therien@sas.upenn.edu

Abstract: We report the synthesis, optical, electrochemical, electronic structural, and transient optical properties of conjugated (porphinato)zinc(II)-spacer-(porphinato)zinc(II) (**PZn-Sp-PZn**) complexes that possess intervening conjugated Sp structures having varying degrees of proquinoidal character. These supermolecular **PZn-Sp-PZn** compounds feature Sp moieties {(4,7-diethynylbenzo[*c*][1,2,5]thiadiazole (**E-BTD-E**), 6,13-diethynylpentacene (**E-PC-E**), 4,9-diethynyl-6,7-dimethyl[1,2,5]thiadiazolo[3,4-*g*]quinoxaline (**E-TDQ-E**), and 4,8-diethynylbenzo[1,2-*c*:4,5-*c*′]bis([1,2,5]thiadiazole) (**E-BBTD-E**)} that regulate frontier orbital energy levels and progressively increase the extent of the quinoidal resonance contribution to the ground and electronically excited states, augmenting the magnitude of electronic communication between terminal (5,-10,20-di(aryl)porphinato)zinc(II) units, relative to that evinced for a bis[(5,5′,-10,20-di(aryl)-porphinato)zinc(II)]butadiyne benchmark (**PZnE-EPZn**). Electronic absorption spectra show significant red-shifts of the respective **PZn-Sp-PZn** x-polarized Q state ($S_0 \rightarrow S_1$) transition manifold maxima (240−4810 cm^{-1}) relative to that observed for **PZnE-EPZn**. Likewise, the potentiometrically determined **PZn-Sp-PZn** HOMO−LUMO gaps ($E_{1/2}{}^{0/+} - E_{1/2}{}^{-/0}$) display correspondingly diminished energy separations that range from 1.88 to 1.11 eV relative to that determined for **PZnE-EPZn** (2.01 eV). Electronic structure calculations provide insight into the origin of the observed **PZn-Sp-PZn** electronic and optical properties. Pump−probe transient spectral data for these **PZn-Sp-PZn** supermolecules demonstrate that the $S_1 \rightarrow S_n$ transition manifolds of these species span an unusually broad spectral domain of the NIR. Notably, the absorption maxima of these $S_1 \rightarrow S_n$ manifolds can be tuned over a 1000−1600 nm spectral region, giving rise to intense excited-state transitions ∼4000 cm^{-1} lower in energy than that observed for the analogous excited-state absorption maximum of the **PZnE-EPZn** benchmark; these data highlight the unusually large quinoidal resonance contribution to the low-lying electronically excited singlet states of these **PZn-Sp-PZn** species. The fact that the length scales of the **PZn-Sp-PZn** species (∼25 Å) are small with respect to those of classic conducting polymers, yet possess NIR $S_1 \rightarrow S_n$ manifold absorptions lower in energy, underscore the unusual electrooptic properties of these conjugated structures.

Introduction

Organic π-conjugated oligomers and polymers constitute a class of promising semiconducting materials having demonstrated utility in device applications ranging from light-emitting diodes,[1,2] photovoltaic cells,[3,4] field-effect transistors,[5,6] to nonlinear optics.[7,8] Reducing and tuning energy gaps between the highest occupied molecular orbital (HOMO) and the lowest unoccupied molecular orbital (LUMO) of such π-conjugated species play crucial roles in optimizing the performance of electronic and optical devices based on active organic components.[9−16]

Porphyrins are tetrapyrrolic conjugated macrocyclic systems that possess modest potentiometrically determined HOMO−LUMO gaps (E_p; $E_{1/2}{}^{0/+} - E_{1/2}{}^{-/0}$) relative to those of the common monomeric aromatic building blocks used to construct traditional electronic polymers. The electronic properties of

(1) Segura, J. L. *Acta Polym.* **1998**, *49*, 319−344.
(2) Mitschke, U.; Bäuerle, P. *J. Mater. Chem.* **2000**, *10*, 1471−1507.
(3) Yu, G.; Gao, J.; Hummelen, J. C.; Wudl, F.; Heeger, A. J. *Science* **1995**, *270*, 1789−1791.
(4) Brabec, C. J.; Sariciftci, N. S.; Hummelen, J. C. *Adv. Funct. Mater.* **2001**, *11*, 15−26.
(5) Katz, H. E. *J. Mater. Chem.* **1997**, *7*, 369−376.
(6) Katz, H. E.; Bao, Z.; Gilat, S. L. *Acc. Chem. Res.* **2001**, *34*, 359−369.
(7) Nalwa, H. S. *Adv. Mater.* **1993**, *5*, 341−358.
(8) Tykwinski, R. R.; Gubler, U.; Martin, R. E.; Diederich, F.; Bosshard, C.; Günter, P. *J. Phys. Chem. B* **1998**, *102*, 4451−4465.
(9) Tour, J. M. *Chem. Rev.* **1996**, *96*, 537−553.
(10) Roncali, J. *Chem. Rev.* **1997**, *97*, 173−205.
(11) van Mullekom, H. A. M.; Vekemans, J. A. J. M.; Meijer, E. W. *Chem. Eur. J.* **1998**, *4*, 1235−1243.
(12) Martin, R. E.; Diederich, F. *Angew. Chem., Int. Ed. Engl.* **1999**, *38*, 1350−1377.
(13) van Mullekom, H. A. M.; Vekemans, J. A. J. M.; Havinga, E. E.; Meijer, E. W. *Mater. Sci. Eng.* **2001**, *32*, 1−40.
(14) Ajayaghosh, A. *Chem. Soc. Rev.* **2003**, *32*, 181−191.
(15) Sonmez, G.; Meng, H.; Wudl, F. *Chem. Mater.* **2003**, *15*, 4923−4929.
(16) Chen, M.; Perzon, E.; Andersson, M. R.; Marcinkevicius, S.; Jönsson, S. K. M.; Fahlman, M.; Berggren, M. *Appl. Phys. Lett.* **2004**, *84*, 3570−3572.

10.1021/ja040243h CCC: $30.25

(porphinato)metal compounds can be modulated extensively by variation of the macrocycle peripheral meso- or β-substituents, as well as by selection of the central metal ion; further, a variety of modes of porphyrinoid−porphyrinoid connectivity provides sufficiently strong interchromophore electronic interactions to facilitate extensive electronic delocalization.[17−42] Of these families of multipigment ensembles that feature substantial ground- and excited-state interchromophore electronic interactions, those that feature direct ethyne-, butadiyne-, and oligoyne-based macrocycle-to-macrocycle connectivity have evinced a wide range of particularly impressive electrooptic properties.[17−24,28−31,36,37] As increasing conjugation length diminishes significantly optical (E_{op}) and potentiometric (E_p) band gaps within these families of structures, multiporphyrin compounds that exploit cylindrically π-symmetric linkers define a point of reference from which to engineer further electronic modulation of conjugated organic materials.

An established means to further reduce the E_{op} and E_p gaps of π-conjugated materials involves introducing quinoid-like character into the conjugation main-chain.[10,13,14] Solution-phase spectroscopic experiments[17,18,21,43] and X-ray crystallographic data[44] obtained for bis[(5,5′,-10,20-di(aryl)porphinato)zinc(II)]-ethyne compounds demonstrate that the bridging ethyne possesses conventional triple bond character in the ground state; electronic absorption,[17,18,20,21] electroabsorption,[20] and pump−probe spectroscopic methods[19,22] are consistent with an excited state electronic structure for this species that features a modest degree of cumulenic (quinoidal) character. Porphyrin-to-porphyrin bridging motifs involving ethynes and spacers that induce a quinoidal structural perturbation with appropriately positioned frontier orbital energy levels, should enhance ground- and excited-state π-conjugation, and effect further reduction in E_{op} and E_p in the corresponding oligomeric and polymeric structures.

Scheme 1

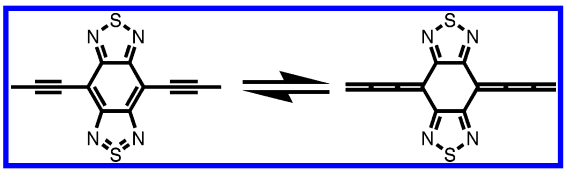

Polymer band-gap reduction through augmentation of π-backbone quinoidal character has been explored both experimentally[45,46] and theoretically.[47,48] In this regard, benzo[1,2-*c*:4,5-*c*′]bis([1,2,5]thiadiazole) (**BBTD**), exemplifies an established conjugated unit with suitable electronic structure to induce substantial quinoidal character in a conjugated backbone.[49−52] Because **BBTD** features large atomic orbital coefficients at its bridging 4- and 8-positions in both the HOMO and LUMO, excellent interchromophore electronic delocalization would be anticipated between [(5,-10,20-di(aryl)porphinato)zinc(II)]ethynyl (**PZnE**) units appended at these positions;[20,21,43,53,54] structural relaxation toward the stable form of **BBTD**'s two 1,2,5-thiadiazole rings would therefore drive an increasing contribution of the cumulenic resonance form to the ground- (S_0) and low-lying electronically excited singlet-state (S_1) wave functions (Scheme 1).[50]

We report the synthesis, optical, electrochemical, and ground- and excited-state electronic structural properties of conjugated (porphinato)zinc(II)-spacer-(porphinato)zinc(II) (**PZn-Sp-PZn**) complexes that feature conjugated Sp structures having varying degrees of proquinoidal character (Figure 1). These Sp moieties {4,7-diethynylbenzo[*c*][1,2,5]thiadiazole (**E-BTD-E**),[55−58] 6,13-diethynylpentacene (**E-PC-E**),[59,60] 4,9-diethynyl-6,7-dimethyl-[1,2,5]thiadiazolo[3,4-*g*]quinoxaline (**E-TDQ-E**), and 4,8-diethynylbenzo[1,2-*c*:4,5-*c*′]bis([1,2,5]thiadiazole) (**E-BBTD-E**)} progressively increase the extent of the cumulenic resonance contribution to the **PZn-Sp-PZn** S_0- and S_1-state structures, and magnify the electronic communication between the component

(17) Lin, V. S.-Y.; DiMagno, S. G.; Therien, M. J. *Science* **1994**, *264*, 1105−1111.
(18) Lin, V. S.-Y.; Therien, M. J. *Chem. Eur. J.* **1995**, *1*, 645−651.
(19) Kumble, R.; Palese, S.; Lin, V. S.-Y.; Therien, M. J.; Hochstrasser, R. M. *J. Am. Chem. Soc.* **1998**, *120*, 11489−11498.
(20) Shediac, R.; Gray, M. H. B.; Uyeda, H. T.; Johnson, R. C.; Hupp, J. T.; Angiolillo, P. J.; Therien, M. J. *J. Am. Chem. Soc.* **2000**, *122*, 7017−7033.
(21) Susumu, K.; Therien, M. J. *J. Am. Chem. Soc.* **2002**, *124*, 8550−8552.
(22) Rubtsov, I. V.; Susumu, K.; Rubtsov, G. I.; Therien, M. J. *J. Am. Chem. Soc.* **2003**, *125*, 2687−2696.
(23) Ostrowski, J. C.; Susumu, K.; Robinson, M. R.; Therien, M. J.; Bazan, G. C. *Adv. Mater.* **2003**, *15*, 1296−1300.
(24) Angiolillo, P. J.; Uyeda, H. T.; Duncan, T. V.; Therien, M. J. *J. Phys. Chem. B* **2004**, *108*, 11893−11903.
(25) Fletcher, J. T.; Therien, M. J. *J. Am. Chem. Soc.* **2000**, *122*, 12393−12394.
(26) Fletcher, J. T.; Therien, M. J. *Inorg. Chem.* **2002**, *41*, 331−341.
(27) Fletcher, J. T.; Therien, M. J. *J. Am. Chem. Soc.* **2002**, *124*, 4298−4311.
(28) Anderson, H. L. *Inorg. Chem.* **1994**, *33*, 972−981.
(29) Taylor, P. N.; Wylie, A. P.; Huuskonen, J.; Anderson, H. L. *Angew. Chem. Int. Ed.* **1998**, *37*, 986−989.
(30) Taylor, P. N.; Huuskonen, J.; Rumbles, G.; Aplin, R. T.; Williams, E.; Anderson, H. L. *Chem. Commun.* **1998**, 909−910.
(31) Arnold, D. P.; Heath, G. A.; James, D. A. *J. Porphyrins Phthalocyanines* **1999**, *3*, 5−31.
(32) Jiang, B.; Yang, S.-W.; Barbini, D. C.; Jones Jr., W. E. *Chem. Commun.* **1998**, 213-214.
(33) Yamamoto, T.; Fukushima, N.; Nakajima, H.; Maruyama, T.; Yamaguchi, I. *Macromolecules* **2000**, *33*, 5988−5994.
(34) Odobel, F.; Suresh, S.; Blart, E.; Nicolas, Y.; Quintard, J.-P.; Janvier, P.; Le Questel, J.-Y.; Illien, B.; Rondeau, D.; Richomme, P.; Häupl, T.; Wallin, S.; Hammarström, L. *Chem. Eur. J.* **2002**, *8*, 3027−0345.
(35) Li, G.; Wang, T.; Schulz, A.; Bhosale, S.; Lauer, M.; Espindola, P.; Heinze, J.; Fuhrhop, J.-H. *Chem. Commun.* **2004**, 552−553.
(36) Beljonne, D.; O'Keefe, G. E.; Hamer, P. J.; Friend, R. H.; Anderson, H. L.; Brédas, J. L. *J. Chem. Phys.* **1997**, *106*, 9439−9460.
(37) Susumu, K.; Maruyama, H.; Kobayashi, H.; Tanaka, K. *J. Mater. Chem.* **2001**, *11*, 2262−2270.
(38) Crossley, M. J.; Govenlock, L. J.; Prashar, J., K. *J. Chem. Soc., Chem. Commun.* **1995**, 2379−2380.
(39) Jaquinod, L.; Siri, O.; Khoury, R. G.; Smith, K. M. *Chem. Commun.* **1998**, 1261−1262.
(40) Vicente, M. G. H.; Cancilla, M. T.; Lebrilla, C. B.; Smith, K. M. *Chem. Commun.* **1998**, 2355−2356.
(41) Tsuda, A.; Osuka, A. *Science* **2001**, *293*, 79−82.
(42) Cho, H. S.; Jeong, D. H.; Cho, S.; Kim, D.; Matsuzaki, Y.; Tanaka, K.; Tsuda, A.; Osuka, A. *J. Am. Chem. Soc.* **2002**, *124*, 14642−14654.
(43) LeCours, S. M.; DiMagno, S. G.; Therien, M. J. *J. Am. Chem. Soc.* **1996**, *118*, 11854−11864.
(44) Uyeda, H. T. Doctoral Dissertation, University of Pennsylvania, Philadelphia, 2002.
(45) Kobayashi, M.; Colaneri, N.; Boysel, M.; Wudl, F.; Heeger, A. J. *J. Chem. Phys.* **1985**, *82*, 5717−5723.
(46) Jenekhe, S. A. *Nature* **1986**, *322*, 345−347.
(47) Brédas, J. L.; Heeger, A. J.; Wudl, F. *J. Chem. Phys.* **1986**, *85*, 4673−4678.
(48) Lee, Y.-S.; Kertesz, M. *J. Chem. Phys.* **1988**, *88*, 2609−2617.
(49) Ono, K.; Tanaka, S.; Yamashita, Y. *Angew. Chem., Int. Ed. Engl.* **1994**, *33*, 1977−1979.
(50) Karikomi, M.; Kitamura, C.; Tanaka, S.; Yamashita, Y. *J. Am. Chem. Soc.* **1995**, *117*, 6791−6792.
(51) Kitamura, C.; Tanaka, S.; Yamashita, Y. *Chem. Mater.* **1996**, *8*, 570−578.
(52) Yamashita, Y.; Ono, K.; Tomura, M.; Tanaka, S. *Tetrahedron* **1997**, *53*, 10169−10178.
(53) LeCours, S. M.; Guan, H.-W.; DiMagno, S. G.; Wang, C. H.; Therien, M. J. *J. Am. Chem. Soc.* **1996**, *118*, 1497−1503.
(54) Priyadarshy, S.; Therien, M. J.; Beratan, D. N. *J. Am. Chem. Soc.* **1996**, *118*, 1504−1510.
(55) Bangcuyo, C. G.; Evans, U.; Myrick, M. L.; Bunz, U. H. F. *Macromolecules* **2001**, *34*, 7592−7594.
(56) Akhtaruzzaman, M.; Tomura, M.; Zaman, M. B.; Nishida, J.-i.; Yamashita, Y. *J. Org. Chem.* **2002**, *67*, 7813−7818.
(57) Yamamoto, T.; Morikita, T. *Macromolecules* **2003**, *36*, 4262−4267.
(58) Kato, S.-i.; Matsumoto, T.; Ishi-i, T.; Thiemann, T.; Shigeiwa, M.; Gorohmaru, H.; Maeda, S.; Yamashita, Y.; Mataka, S. *Chem. Commun.* **2004**, 2342−2343.
(59) Anthony, J. E.; Brooks, J. S.; Eaton, D. L.; Parkin, S. R. *J. Am. Chem. Soc.* **2001**, *123*, 9482−9483.
(60) Anthony, J. E.; Eaton, D. L.; Parkin, S. R. *Org. Lett.* **2002**, *4*, 15−18.

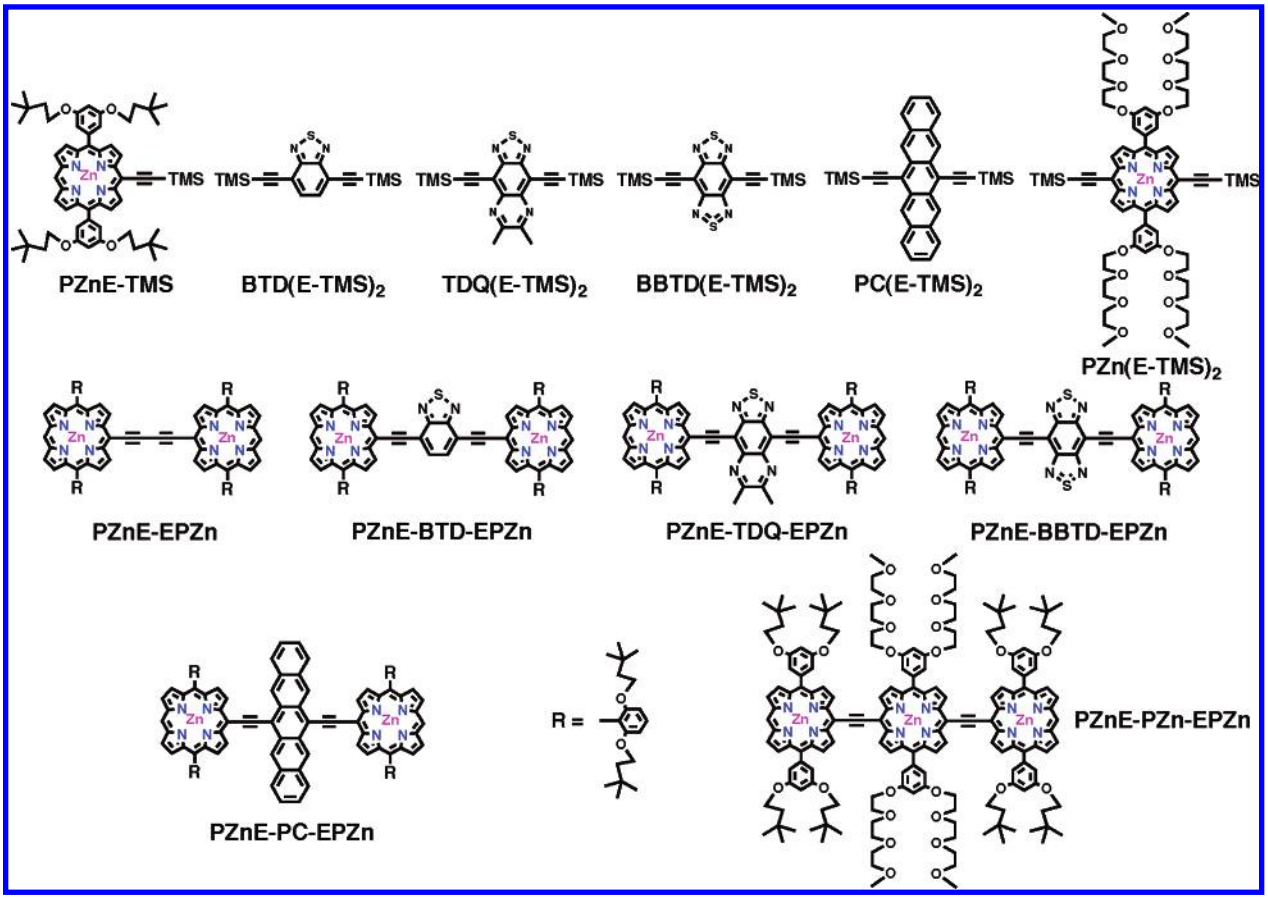

Figure 1. Structures of the bis[(porphinato)zinc(II)] derivatives **PZnE-EPZn**, **PZnE-BTD-EPZn**, **PZnE-PC-EPZn**, **PZnE-TDQ-EPZn**, and **PZnE-BBTD-EPZn** along with key reference compounds.

PZnE units relative to that evinced for a bis[(5,5′,-10,20-di-(aryl)porphinato)zinc(II)]butadiyne benchmark (**PZnE-EPZn**). Electronic structural differences, as well as the relative magnitudes of the optical (E_{op}) and potentiometric (E_p) band gaps of these new conjugated **PZn-Sp-PZn** structures are rationalized within the context of perturbation theory.

Experimental Section

Materials. Synthetic procedures and characterization data for new compounds [4,7-bis[(10,20-bis[2′,6′-bis(3,3-dimethyl-1-butyloxy)phenyl]porphinato)zinc(II)-5-ylethynyl]benzo[*c*][1,2,5]thiadiazole (**PZnE-BTD-EPZn**), 6,13-bis[(10,20-bis[2′,6′-bis(3,3-dimethyl-1-butyloxy)-phenyl]porphinato)zinc(II)-5-ylethynyl]pentacene (**PZnE-PC-EPZn**), 4,9-bis[(10,20-bis[2′,6′-bis(3,3-dimethyl-1-butyloxy)phenyl]porphinato)-zinc(II)-5-ylethynyl]-6,7-dimethyl[1,2,5]thiadiazolo[3,4-*g*]quinoxaline (**PZnE-TDQ-EPZn**), 4,8-bis[(10,20-bis[2′,6′-bis(3,3-dimethyl-1-butyl-oxy)phenyl]porphinato)zinc(II)-5-ylethynyl]benzo[1,2-*c*:4,5-*c*′][1,2,5]-bis([1,2,5]thiadiazole) (**PZnE-BBTD-EPZn**)] are given in the Supporting Information.

Instrumentation. Electronic absorption spectra were recorded on an OLIS UV/vis/near-IR spectrophotometry system that is based on the optics of a Cary 14 spectrophotometer. NMR spectra were recorded on 360 MHz DMX-360 or 300 MHz DMX-300 Brüker spectrometers. Cyclic voltammetric measurements were carried out on an EG&G Princeton Applied Research model 273A Potentiostat/Galvanostat. The electrochemical cell used for these experiments utilized a platinum disk working electrode, a platinum wire counter electrode, and a saturated calomel reference electrode (SCE). The reference electrode was separated from the bulk solution by a junction bridge filled with the corresponding solvent/supporting electrolyte solution. The ferrocene/ferrocenium redox couple was utilized as an internal potentiometric standard.

Electronic Structure Calculations. All electronic structure calculations were carried out using the GAUSSIAN 98 programs.[61] Geometry optimizations and semiempirical electronic structural calculations were performed using the PM3 method. To minimize computational effort, the solubilizing alkoxy substituents of the **PZn-Sp-PZn** structures, the **PZnE** trimethylsilyl group, and the methyl groups of 6,7-dimethyl-[1,2,5]thiadiazolo[3,4-g]quinoxaline were replaced by hydrogen. Structural models for **PZnE-EPZn**, **PC**, **BBTD**, **PZnE-PC-EPZn**, and **PZnE-BBTD-EPZn** were optimized within D_{2h} constraints, while optimal **PZnE**, **BTD**, **TDQ**, **PZnE-BTD-EPZn** and **PZnE-TDQ-EPZn** structures were computed for C_{2v} symmetry. Orbital contour plots were visualized with the gOpenMol program.[62]

Ultrafast Transient Absorption Experiments. Experimental details are provided in the Supporting Information.

Results and Discussion

Synthesis. Structures of the **PZn-Sp-PZn** supermolecules along with related ethynylated Sp and PZn reference compounds

(61) Frisch, M. J.; Trucks, G. W.; Schlegel, H. B.; Scuseria, G. E.; Robb, M. A.; Cheeseman, J. R.; Zakrzewski, V. G.; Montgomery, J. A.; Stratmann, R. E.; Burant, J. C.; Dapprich, S.; Millam, J. M.; Daniels, A. D.; Kudin, K. N.; Strain, M. C.; Farkas, O.; Tomasi, J.; Barone, V.; Cossi, M.; Cammi, R.; Mennucci, B.; Pomelli, C.; Adamo, C.; Clifford, S.; Ochterski, J.; Petersson, G. A.; Ayala, P. Y.; Cui, Q.; Morokuma, K.; Malick, D. K.; Rabuck, A. D.; Raghavachari, K.; Foresman, J. B.; Cioslowski, J.; Ortiz, J. V.; Stefanov, B. B.; Liu, G.; Liashenko, A.; Piskorz, P.; Komaromi, I.; Gomperts, R.; Martin, R. L.; Fox, D. J.; Keith, T.; Al-Laham, M. A.; Peng, C. Y.; Nanayakkara, A.; Gonzalez, C.; Challacombe, M.; Gill, P. M. W.; Johnson, B. G.; Chen, W.; Wong, M. W.; Andres, J. L.; Head-Gordon, M.; Replogle, E. S.; Pople, J. A. *Gaussian 98*, Revision A.9; Gaussian, Inc: Pittsburgh, PA, 1998.

are shown in Figure 1. These **PZn-Sp-PZn** species were synthesized by palladium (Pd)-mediated cross-coupling reactions involving appropriately substituted (porphinato)zinc(II) (PZn) compounds and Sp units (see Supporting Information). The PZn-containing structures of Figure 1 exploit 2′,6′-bis(3,3-dimethyl-1-butyloxy)phenyl groups as 10- and 20-*meso*-porphyrin substituents, which facilitate excellent solubility and straightforward assignment of ^{1}H NMR spectra.[21,63] 4,7-Diethynylbenzo[*c*][1,2,5]thiadiazole (**E-BTD-E**), 6,13-diethynylpentacene (**E-PC-E**), 4,9-diethynyl-6,7-dimethyl[1,2,5]thiadiazolo[3,4-*g*]quinoxaline (**E-TDQ-E**), and 4,8-diethynylbenzo[1,2-*c*:4,5-*c*′]bis([1,2,5]thiadiazole) (**E-BBTD-E**) were selected as proquinodal Sp units.

The nature of the functionalized PZn and Sp moieties used in the synthesis of the corresponding **PZn-Sp-PZn** complexes varied with Sp electronic structure. For the **PZn-Sp-PZn** structure featuring a **E-BTD-E** Sp unit (**PZnE-BTD-EPZn**, Figure 1), the coupling reaction between (5-ethynyl-10,20-bis[2′,6′-bis(3,3-dimethyl-1-butyloxy)phenyl]porphinato)zinc(II) and 4,7-dibromobenzo[*c*][1,2,5]thiadiazole gave a mixture of products that included not only the target molecule, but also the butadiyne-bridged bis[(porphinato)zinc(II)] complex (**PZnE-EPZn**). As these two species were difficult to separate by both silica gel and size exclusion column chromatography under the conditions employed, **PZnE-BTD-EPZn** was synthesized via a Pd-mediated coupling reaction involving (5-iodo-10,20-bis[2′,6′-bis(3,3-dimethyl-1-butyloxy)phenyl]porphinato)zinc(II) and 4,7-bis(trimethylsilylethynyl)benzo[*c*][1,2,5]thiadiazole in which in situ deprotection of the trimethylsilyl (TMS) group with K_2CO_3 was utilized. An identical in situ deprotection strategy was utilized in the synthesis of **PZnE-PC-EPZn**, as 6,13-diethynylpentacene (**E-PC-E**) possesses low solubility. Respective **PZn-Sp-PZn** complexes utilizing thiadiazoloquinoxaline and benzobis(thiadiazole) moieties as Sp components (**PZnE-TDQ-EPZn** and **PZnE-BBTD-EPZn**, Figure 1) were synthesized successfully from (5-ethynyl-10,20-bis[2′,6′-bis(3,3-dimethyl-1-butyloxy)phenyl]porphinato)zinc(II) and the corresponding dibromo proquinoid spacer derivatives, as trace **PZnE-EPZn** contaminants could easily be separated from the **PZn-Sp-PZn** product by silica gel column chromatography.

Steady-State Absorption Spectra. Electronic absorption spectra for the **PZn-Sp-PZn** complexes, along with the spectrum for the bis[(5,5′,-10,20-di(aryl)porphinato)zinc(II)]butadiyne (**PZnE-EPZn**) benchmark, are displayed in Figure 2. Analogous electronic spectra for trimethylsilyl-protected analogues of proquinoidal Sp reference compounds **E-BTD-E**, **E-PC-E**, **E-TDQ-E**, and **E-BBTD-E**, as well as comprehensive tabulated electronic absorption spectral data, are contained in the Supporting Information. As expected for the mode of porphyrin-to-porphyrin connectivity and the nature of the conjugated components, extensive electronic interactions are manifest between the PZn and Sp components of these structures.[17−22] The electronic absorption spectrum for **PZnE-EPZn** (Figure 2A), as well as the linear electronic spectra of these **PZn-Sp-PZn** compounds (Figure 2B−E), are dominated by two absorption manifolds derived from the classic porphyrin B (Soret) ($S_0 \rightarrow S_2$) and Q-band ($S_0 \rightarrow S_1$) transitions. The gross spectral features of these species evince the hallmarks of extensive π conjugation and exciton coupling, and have been analyzed in detail for a wide-range of structurally related compounds.[17−22]

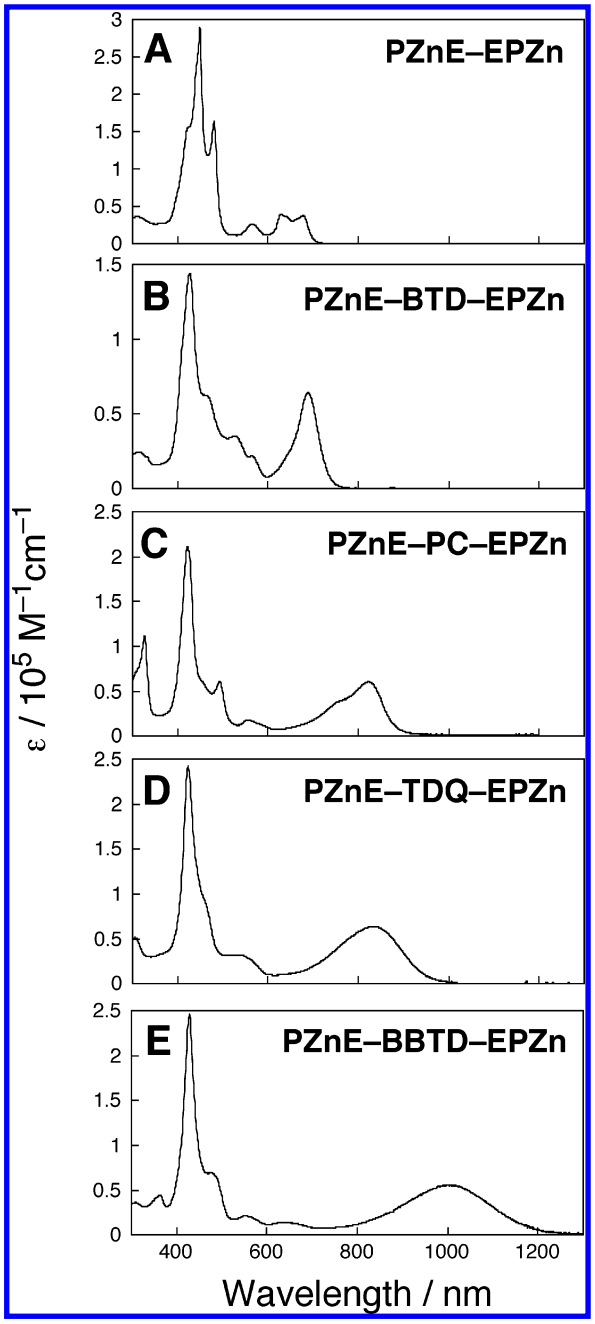

Figure 2. Electronic absorption spectra of: (A) **PZnE-EPZn**, (B) **PZnE-BTD-EPZn**, (C) **PZnE-PC-EPZn**, (D) **PZnE-TDQ-EPZn**, and (E) **PZnE-BBTD-EPZn** recorded in THF solvent.

The Soret band regions of these **PZn-Sp-PZn** compounds show splittings characteristic of extensive excitonic interactions.[64] Note that the **PZnE-BTD-EPZn**, **PZnE-PC-EPZn**, **PZnE-TDQ-EPZn**, and **PZnE-BBTD-EPZn** spectra (Figure 2) display a sharp B-state absorption close in energy to that of 5-ethynyl(porphinato)zinc(II) reference compound (**PZnE-TMS**, Figure 1; see Supporting Information); interestingly, this high energy component of the B-state manifold of these compounds displays less structure than that observed in the **PZnE-EPZn** spectrum (Figure 2A). Congruent with the body of spectroscopic

(62) Laaksonen, L. *gOpenMol*, Version 2.0; Espoo, Finland, 2001.
(63) Uyeda, H. T.; Zhao, Y.; Wostyn, K.; Asselberghs, I.; Clays, K.; Persoons, A.; Therien, M. J. *J. Am. Chem. Soc.* **2002**, *124*, 13806−13813.
(64) Kasha, M.; Rawls, H. R.; El-Bayoumi, M. A. *Pure Appl. Chem.* **1965**, *11*, 371−392.

Table 1. Comparative Integrated Oscillator Strengths and Absorptive Domains of the Blue and Red Spectral Regions of Conjugated Porphyrin Dimers Relative to the **PZnE-TMS** Benchmark[a]

compound	FWHM[b] B-band region [cm^{-1}, (nm)]		oscillator strength B-band region[d]	FWHM[e] Q-band region [cm^{-1}, (nm)]		oscillator strength Q-band region[f]	total oscillator strength[g]
PZnE-TMS	696	(428)	1.059	756	(562)	0.062	1.121
				457	(603)		
PZnE-EPZn	1976	(449)[c]	3.643	1512	(566)	0.467	5.197
	592	(481)[c]		588	(628)		
				536	(678)		
PZnE-BTD-EPZn	2323	(426)[c]	2.108	1180	(689)	0.719	3.519
PZnE-PC-EPZn	1745	(421)	2.667	1992	(823)	0.737	5.456
	1014	(493)[c]					
PZnE-TDQ-EPZn	1945	(423)	3.076	2510	(839)	1.144	5.515
PZnE-BBTD-EPZn	1623	(429)	2.803	2341	(1006)	0.972	5.167
	2053	(479)[c]					

[a] From electronic absorption spectra recorded in THF solvent. [b] Taken as the spectral width of the B-band region at half the height of the absorption noted. [c] Taken as twice value of half the spectral width of the B-band region at half the height of the absorption noted. [d] Oscillator strengths calculated over the following wavelength domains: **PZnE-TMS** (360∼470 nm); **PZnE-EPZn** (360∼530 nm); **PZnE-BTD-EPZn** (360∼510 nm); **PZnE-PC-EPZn** (360∼535 nm); **PZnE-TDQ-EPZn** (360∼510 nm); **PZnE-BBTD-EPZn** (380∼525 nm). [e] Entries correspond to the spectral breadth of the transition envelope centered at the wavelength in parentheses. [f] Oscillator strengths calculated over the following wavelength domains: **PZnE-TMS** (470∼650 nm); **PZnE-EPZn** (530∼750 nm); **PZnE-BTD-EPZn** (510∼850 nm); **PZnE-PC-EPZn** (535∼1000 nm); **PZnE-TDQ-EPZn** (510∼1000 nm); **PZnE-BBTD-EPZn** (525∼1400 nm). [g] Oscillator strengths calculated over the following wavelength domains: **PZnE-TMS** (360∼650 nm); **PZnE-EPZn** (280∼750 nm); **PZnE-BTD-EPZn** (280∼850 nm); **PZnE-PC-EPZn** (280∼1000 nm); **PZnE-TDQ-EPZn** (280∼1100 nm); **PZnE-BBTD-EPZn** (280∼1400 nm).

Table 2. Prominent Absorption Band Wavelength, Energies, and Extinction Coefficients of Conjugated **PZn-Sp-PZn** Compounds Relative to the **PZnE-TMS** Benchmark in THF Solvent

compound	UV-region			B-band region			Q-band region		
	λ(nm)	ν(cm^{-1})	log(ϵ)	λ(nm)	ν(cm^{-1})	log(ϵ)	λ(nm)	ν(cm^{-1})	log(ϵ)
PZnE-TMS				428	23,364	(5.53)	562	17,794	(4.17)
							603	16,584	(3.92)
PZnE-EPZn	308	32468	(4.56)	423	23,640	(5.19)	566	17,668	(4.42)
				449	22,272	(5.46)	628	15,924	(4.60)
				481	20,790	(5.21)	678	14,749	(4.58)
PZnE-BTD-EPZn	313	31949	(4.39)	426	23,474	(5.16)	524	19,084	(4.55)
				465	21,505	(4.79)	566	17,668	(4.34)
							689	14,514	(4.81)
PZnE-PC-EPZn	326	30675	(5.05)	421	23,753	(5.32)	555	18,018	(4.26)
				493	20,284	(4.79)	823	12,151	(4.78)
PZnE-TDQ-EPZn	305	32,787	(4.71)	423	23,641	(5.38)	531	18,832	(4.51)
							839	11,919	(4.80)
PZnE-BBTD-EPZn	308	32,468	(4.56)	429	23,310	(5.39)	551	18,149	(4.33)
	363	27,548	(4.65)	479	20,877	(4.84)	638	15,674	(4.16)
							1006	9,940	(4.75)

data obtained for **PZnE-EPZn** and related ethyne- and butadiyne-bridged bis(PZn) compounds,[17−22,28,36,65,66] this spectral signature reflects the diminished y-polarized B-state dipolar interaction (y taken orthogonal to the highly conjugated axis of the structure) that occurs with increasing PZn−PZn distance for the **PZnE-BTD-EPZn**, **PZnE-PC-EPZn**, **PZnE-TDQ-EPZn**, and **PZnE-BBTD-EPZn** supermolecules, consistent with expectations based on the point-dipole approximation of the general exciton model originally developed by Kasha.[64] In contrast, the low energy, x-polarized B-state transitions along the vector defined by the ethyne moieties of these **PZn-Sp-PZn** compounds are markedly reduced in absolute intensity with respect to the B_x band centered at 481 nm in the **PZnE-EPZn** spectrum, and are observed to be less significant relative to their respective prominent y-polarized B-state absorptions (Figure 2, Table 2).

This decrease in x-polarized B-state oscillator strength observed in the Figure 2 spectra for **PZnE-BTD-EPZn**, **PZnE-PC-EPZn**, **PZnE-TDQ-EPZn**, and **PZnE-BBTD-EPZn** relative to that manifest for **PZnE-EPZn**, reflects enhanced B_x-state intensity borrowing by the corresponding Q-state absorptions driven by the proquinoidal PZn-to-PZn bridging units.[20,67] This augmentation of x-polarized Q-state absorption oscillator strength increases concomitantly with the ability of the S_0 and S_1 states of these species to delocalize charge (Tables 1 and 2, vide infra),[17,18,21] and tracks with the magnitude of the Q_x absorption wavelength [Compound, (λ_{max}(Q_x band)): **PZnE-EPZn** (678 nm), **PZnE-BTD-EPZn** (689 nm), **PZnE-PC-EPZn** (823 nm), **PZnE-TDQ-EPZn** (839 nm) and **PZnE-BBTD-EPZn** (1006 nm)]. Note that the full spectral width at half-maximum (fwhm) of the Q_x-state absorption manifold follows a similar trend with **PZnE-EPZn** < **PZnE-BTD-EPZn** < **PZnE-PC-EPZn** < **PZnE-TDQ-EPZn** ∼ **PZnE-BBTD-EPZn** (Figure 2, Table 1). In this regard, note that the Q_x manifold spectral band shapes for **PZnE-TDQ-EPZn** and **PZnE-BBTD-EPZn** tail extensively at low energy, with the **PZnE-BBTD-EPZn** spectrum displaying measurable oscillator strength well beyond 1200 nm (Figure

(65) Angiolillo, P. J.; Lin, V. S.-Y.; Vanderkooi, J. M.; Therien, M. J. *J. Am. Chem. Soc.* **1995**, *117*, 12514−12527.
(66) O'Keefe, G. E.; Denton, G. J.; Harvey, E. J.; Phillips, R. T.; Friend, R. H.; Anderson, H. L. *J. Chem. Phys.* **1996**, *104*, 805−811.
(67) Gouterman, M. In *The Porphyrins*; Dolphin, D., Ed.; Academic Press: London, 1978; Vol. III, p 1−165.

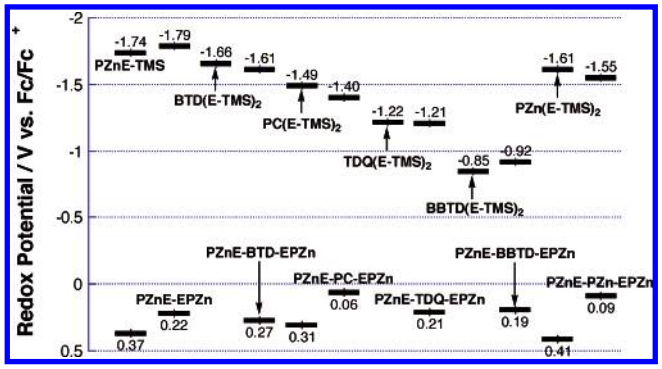

Figure 3. Schematic highlighting the potentiometrically determined HOMO and LUMO energy levels of the **PZn-Sp-PZn** complexes relative to those of ethyne-functionalized PZn and proquinoidal Sp moieties. Redox potentials shown are relative to the ferrocene/ferrocenium (Fc/Fc^+) redox couple, which was used as an internal standard in these experiments.

2). Absorption wavelengths, energies, and extinction coefficients for the prominent transitions of these compounds are tabulated in Table 2.

Electrochemical Properties. Figure 3 highlights the potentiometrically determined HOMO and LUMO energy levels of the **PZn-Sp-PZn** complexes relative to those of ethyne-functionalized PZn and proquinoidal Sp moieties, **PZnE-EPZn**, and a related tris[(porphinato)zinc(II)] complex, (5,15-bis-[[(5′,-10′,20′-bis[3,5-di(3,3-dimethyl-1-butyloxy)phenyl]porphinato)-zinc(II)]ethynyl]-10,20-bis[3,5-di(9-methoxy-1,4,7-trioxanonyl)-phenyl]porphinato)zinc(II) (**PZnE-PZn-EPZn**).[17,21] The cyclic voltammetric data shown in this figure highlight a number of electronic structural features of these **PZn-Sp-PZn** species. **PZn-Sp-PZn** $E_{1/2}{}^{0/+}$ values vary modestly with Sp electronic structure over a 0.21 eV range, with HOMO level destabilization increasing in the order **PZnE-BTD-EPZn** < **PZnE-EPZn** ∼ **PZnE-TDQ-EPZn** < **PZnE-BBTD-EPZn** < **PZnE-PC-EPZn** (Figure 3). In contrast, measured **PZn-Sp-PZn** $E_{1/2}{}^{-/0}$ values span a 0.87 eV potentiometric domain, mirroring closely the relative changes observed for $E_{1/2}{}^{-/0}$ determined for their corresponding trimethylsilyl-elaborated Sp [Sp(E-TMS)$_2$] structures, and evincing LUMO level stabilization that escalates in the order **PZnE-EPZn** < **PZnE-BTD-EPZn** < **PZnE-PC-EPZn** < **PZnE-TDQ-EPZn** < **PZnE-BBTD-EPZn**. This strong dependence of **PZn−Sp-PZn** $E_{1/2}{}^{-/0}$ values upon the nature of the building block ethyne-elaborated Sp moiety plays the predominant role in determining the magnitude of the potentiometrically determined HOMO−LUMO gaps (E_p; $E_{1/2}{}^{0/+} - E_{1/2}{}^{-/0}$) within this series of supermolecular bis(PZn) compounds that feature proquinoidal Sp units [Compound, (E_p): **PZnE-EPZn** (2.01 eV), **PZnE-BTD-EPZn** (1.88 eV), **PZnE-PC-EPZn** (1.46 eV), **PZnE-TDQ-EPZn** (1.42 eV) and **PZnE-BBTD-EPZn** (1.11 eV); see Figure 3, Table 3]. Note that despite augmented PZn-to-PZn centroid-to-centroid distances, the magnitudes of the potentiometrically evaluated HOMO−LUMO gaps for these **PZn-Sp-PZn** structures are markedly diminished relative to the **PZnE-EPZn** benchmark. Further, given that **PZnE-PZn-EPZn**[21] can be considered a bis(PZn) complex bridged by a 5,15-diethynyl(porphinato)zinc(II) ($PZnE_2$) Sp moiety, the fact that E_p for this structure (Figure 3) exceeds that determined for **PZnE-TDQ-EPZn**, **PZnE-PC-EPZn**, and **PZnE-BBTD-EPZn**, demonstrates that proquinoidal Sp electronic structure, in contrast to Sp π-aromatic size, can be the more important determinant of the extent of π-conjugation in π-conjugated oligomers and polymers.

While the magnitudes of **PZnE-BTD-EPZn** and **PZnE-PC-EPZn** E_p values suggest respective HOMOs and LUMOs that feature substantial conjugative interactions between the PZn, Sp, and ethyne units (Figure 3), the highly stabilized LUMOs of **PZnE-TDQ-EPZn** and **PZnE-BBTD-EPZn** are unusual: note that the **PZnE-TDQ-EPZn** and **PZnE-BBTD-EPZn** one-electron reduction potentials resemble those obtained respectively for **TDQ(E-TMS)$_2$** and **BBTD(E-TMS)$_2$**, potentially indicating that radical anion state electron density is largely localized on the Sp fragments of these **PZn-Sp-PZn** supermolecules. While electronic structure calculations provide further insight into this matter, it is important to note that the optical band gaps (E_{op} values) of **PZnE-BTD-EPZn**, **PZnE-PC-EPZn**, **PZnE-TDQ-EPZn**, and **PZnE-BBTD-EPZn** track closely with their corresponding E_ps (Figures 2−3, Tables 2−3). These data, coupled with the facts that: (i) the steady-state absorption spectra indicate that the visible and NIR x-polarized excitations feature extensive mixing of PZn- and Sp-derived electronic states, and (ii) the magnitude of the LUMO-level stabilization in the **PZnE-BTD-EPZn**, **PZnE-PC-EPZn**, **PZnE-TDQ-EPZn**, and **PZnE-BBTD-EPZn** series is extensive with respect to the corresponding HOMO-level destabilization evinced in these structures, suggest that the quinoidal resonance contribution to the low lying singlet electronically excited states exceeds greatly that for the ground-state, thus giving rise to the expectation that the excited singlet wave functions of these **PZn-Sp-PZn** compounds should feature unusual degrees of electronic delocalization (vide infra).

Electronic Structure Calculations. Further insight into the electrooptic properties of these supermolecules can be garnered from an electronic structural analysis of **PZn-Sp-PZn** frontier orbitals (FOs) as a function of the intervening proquinoidal Sp moiety. Figures 4−8 display respectively the FOs of **PZnE-EPZn**, **PZnE-BTD-EPZn**, **PZnE-PC-EPZn**, **PZnE-TDQ-EPZn**, and **PZnE-BBTD-EPZn**. In these electronic structure calculations, geometry optimizations and semiempirical electronic structural calculations were performed using the PM3 method. Models for the **PZn-Sp-PZn** structures that featured planar macrocycles and Sp units constrained to lie in a common molecular plane, were utilized in the geometrical optimizations. **PZn-Sp-PZn** FOs presented in Figures 4−8 are depicted in an orbital correlation diagram format that shows the corresponding FOs and energies of their respective component PZnE and Sp building blocks. Figure 9 displays the relative calculated HOMO and LUMO energies of all the Figures 4−8 model compounds.

The FOs of **PZnE-EPZn** (Figure 4) resemble those computed for meso-to-meso ethyne-bridged bis(PZn) (**PZn-E-PZn**):[20,21,36,37] (i) the HOMO exhibits substantial butadiyne-, C_{meso}-, and N-centered electron density, with the C_{meso} carbons that constitute a portion of the conjugated macrocycle-to-macrocycle bridge displaying substantial π overlap with their respective C_α carbons; (ii) the LUMO manifests similarly comprehensive electronic delocalization, exhibiting extensive cumulenic character along the C_2 axis defined by the butadiyne moiety. The evolution of FO electron density distributions in bis(porphyrin) compounds that feature a meso-to-meso linkage topology and a cylindrically π-symmetric bridge, relative to classic monomeric porphyrin building blocks, has been discussed in detail.[20] Note

Table 3. Optical HOMO−LUMO Gaps (E_{opS}) and Potentiometrically Determined HOMO−LUMO Gaps (E_{pS}) of the **PZn-Sp-PZn** Complexes Relative to Those of Ethyne-functionalized **PZn** and Proquinoidal **Sp** Moieties

	PZnE-TMS	PZnE-EPZn	BTD(E-TMS)$_2$	PZnE-BTD-EPZn	PC(E-TMS)$_2$	PZnE-PC-EPZn	TDQ(E-TMS)$_2$	PZnE-TDQ-EPZn	BBTD(E-TMS)$_2$	PZnE-BBTD-EPZn
E_{op}(max)[a]	2.06	1.83	3.25	1.80	1.94	1.51	2.46	1.48	2.18	1.23
E_{op}(edge)[b]	2.01	1.77	2.95	1.69	1.89	1.41	2.31	1.31	2.01	1.05
E_p[c]	2.11	2.01	d	1.88	1.80	1.46	d	1.42	d	1.11

[a] Optical HOMO−LUMO gap determined from the lowest absorption maximum measured in THF. [b] Optical HOMO−LUMO gap determined from the absorption edge measured in THF. The absorption edge is defined as the wavelength on the red side of the lowest energy absorption band where the slope changes abruptly. [c] Potentiometrically determined HOMO−LUMO gap ($E_{1/2}^{0/+} - E_{1/2}^{-/0}$) measured in CH_2Cl_2. [d] Irreversible oxidation; value not determined.

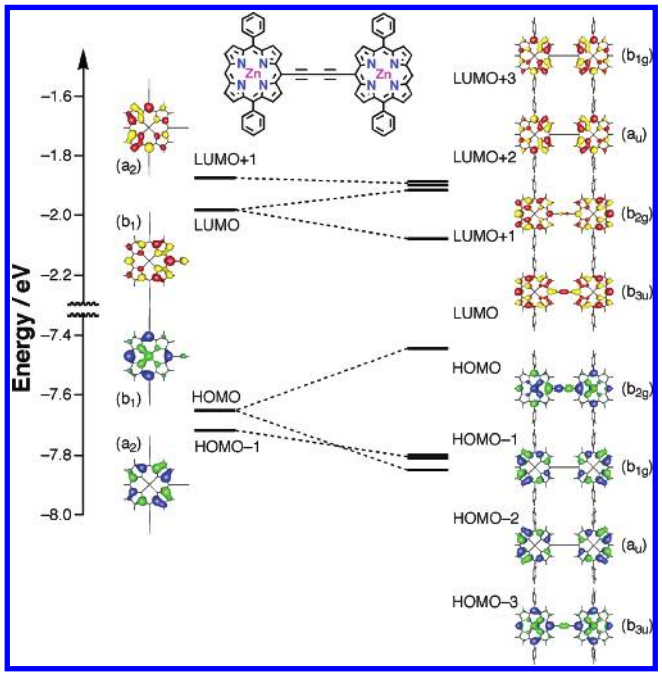

Figure 4. Frontier orbital correlation diagram for **PZnE** and **PZnE-EPZn**.

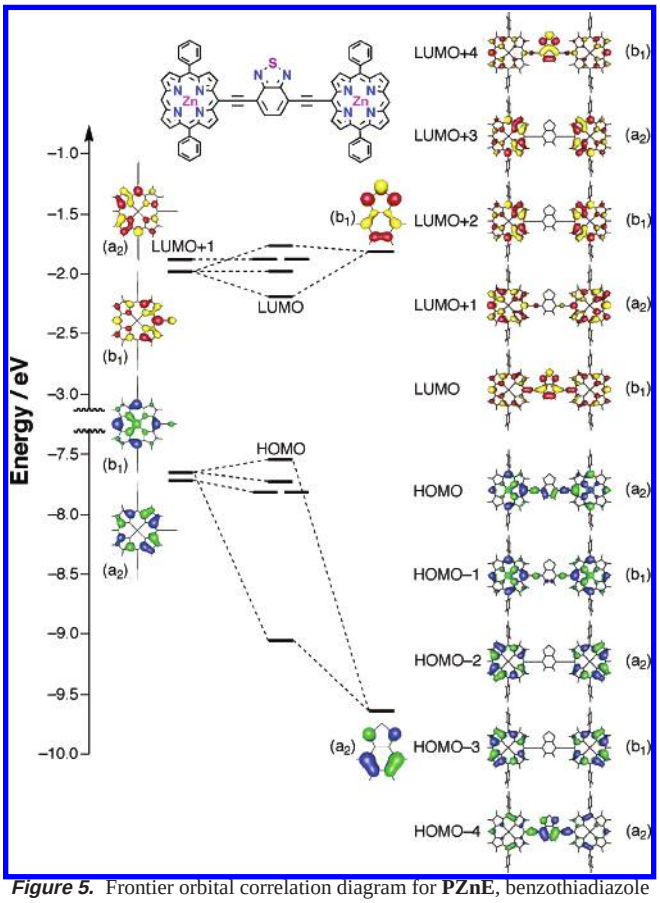

Figure 5. Frontier orbital correlation diagram for **PZnE**, benzothiadiazole (**BTD**), and **PZnE-BTD-EPZn**.

that both the **PZnE-EPZn** electron density distribution within the frontier orbital set, and the magnitude of the energy separation between these orbitals, are consistent with the x-polarized nature of its low lying electronically excited state.[17−27] The **PZnE-EPZn** HOMO is 0.206 eV destabilized with respect to that of the **PZnE** benchmark, whereas its LUMO is 0.098 eV stabilized relative to this ethyne-elaborated monomer. This diminished computed HOMO−LUMO gap for **PZnE-EPZn** relative to **PZnE** is larger than that calculated for **PZn-E-PZn**,[20,21] consistent with the expectation, and extensive spectroscopic evidence indicating, that interporphyryl electronic interactions diminish with increasing macrocycle-macrocycle distances.

An analogous computational study carried out on **PZnE-BTD-EPZn** evinces both a delocalized HOMO and LUMO (Figure 5), similar to that noted for **PZnE-EPZn**. The **PZnE-BTD-EPZn** HOMO illustrates antibonding interactions between the PZn, ethyne, and BTD units that define the highly conjugated axis of the supermolecule, while the LUMO features an extensive degree of quinoidal character, with bonding interactions between the PZn−C_{meso} and ethyne C_α-carbon atoms, antibonding interactions between the ethyne C_α and C_β atoms, and bonding interactions between the ethyne C_β and benzothiadiazole 4- and 7-carbon atoms. The HOMO energy level of **PZnE-BTD-EPZn** is destabilized by 0.106 eV relative to that of **PZnE**, while its LUMO energy level is stabilized by 0.203 eV with respect to this benchmark.

PZnE-PC-EPZn displays FO electron density distributions similar to that noted for **PZnE-BTD-EPZn**, with substantial electronic interactions evident between **PZnE** and **PC** Sp moieties in both the HOMO and LUMO (Figure 6). The energy to which the **PZnE-PC-EPZn** HOMO is destabilized relative to **PZnE** (0.499 eV) has increased with respect to that observed for **PZnE-BTD-EPZn**; likewise, the **PZnE-PC-EPZn** LUMO is considerably more stabilized (0.251 eV, Figure 9) than that computed for **PZnE-BTD-EPZn**. Note in this regard that both (i) large atomic orbital coefficients at the porphyrin meso- and pentacene 6,13-carbon positions in **PZnE-PC-EPZn**, and (ii) excellent energy matching within the **PZnE** and **PC** FO sets drive these substantial HOMO and LUMO energy level perturbations relative to that observed for the **PZnE-BTD-EPZn** case.

The energy difference between the **PZnE** and Sp LUMOs increases as the Sp fragment LUMO energy levels become

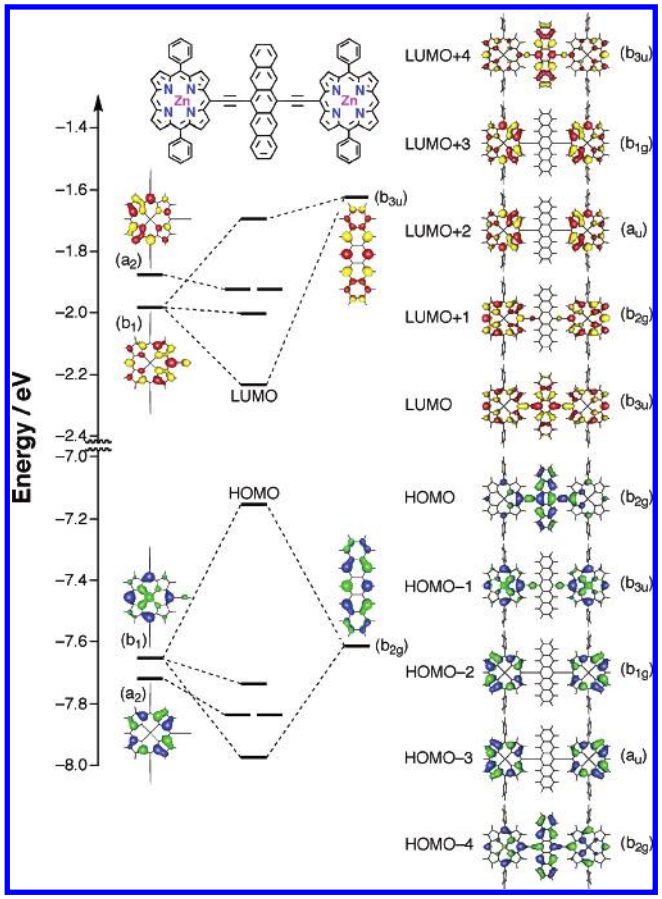

Figure 6. Frontier orbital correlation diagram for **PZnE**, pentacene (**PC**), and **PZnE-PC-EPZn**.

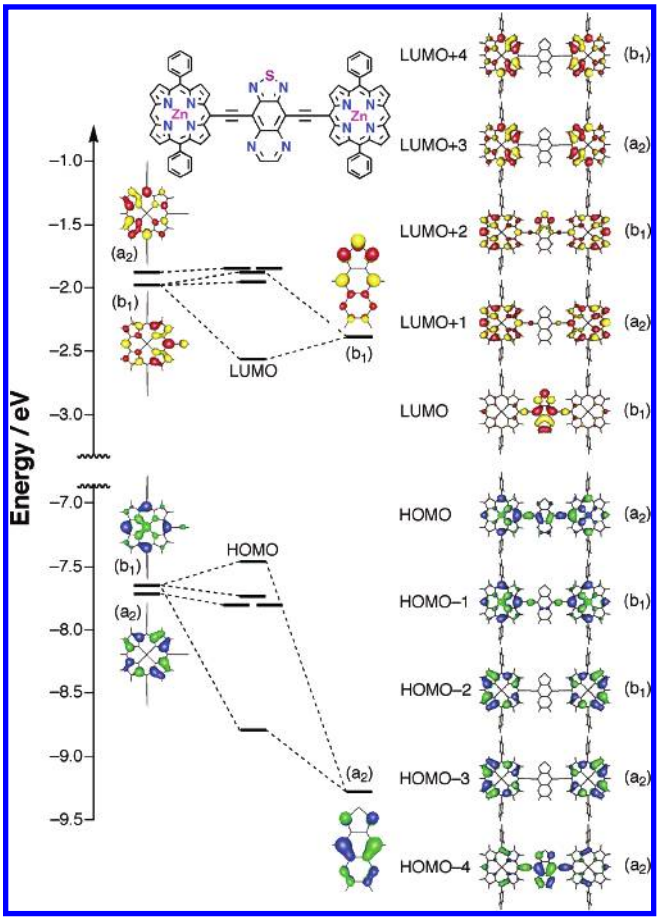

Figure 7. Frontier orbital correlation diagram for **PZnE**, thiadiazoloquinoxaline (**TDQ**), and **PZnE-TDQ-EPZn**.

increasingly stabilized ($|E_{LUMO}(PZnE) - E_{LUMO}(Sp)| = 0.171$ (**PZnE**/**BTD**), 0.356 (**PZnE**/**PC**), 0.407 (**PZnE**/**TDQ**), 1.232 (**PZnE**/**BBTD**) eV; Figures 4−9). Given that the extent of the orbital interaction is inversely proportional to the energy difference between the interacting orbitals,[68] this orbital energy mismatch attenuates the extent of LUMO delocalization in these **PZn-Sp-PZn** supermolecules, causing the LUMO to become increasingly localized on the Sp unit. Thus, while contour plots of the **PZnE-BTD-EPZn**, **PZnE-PC-EPZn**, **PZnE-TDQ-EPZn**, and **PZnE-BBTD-EPZn** HOMOs all show global delocalization, significant LUMO delocalization is evident only in **PZnE-BTD-EPZn** and **PZnE-PC-EPZn** (Figures 5 and 6), with **PZnE-TDQ-EPZn** and **PZnE-BBTD-EPZn** showing highly Sp-localized LUMOs (Figures 7 and 8). Note that the relative calculated HOMO and LUMO energy levels shown in Figure 9 mirror the differences in the potentiometrically determined **PZn-Sp-PZn** HOMO and LUMO energy levels (Figure 3). While these computational and electrochemical data underscore the cardinal role that **PZnE** and Sp fragment orbital energy differences play in fixing the radical cation and anion state energy levels in these **PZn-Sp-PZn** structures, it is important to appreciate that in contrast to many simple conjugated organic building blocks, whose low-lying excited states are described adequately by one-electron transitions, extensive configuration interaction (CI) is necessary to describe correctly porphyrin electronically excited states.[21,67] While absolute HOMO and LUMO energies largely determine $E_{1/2}^{0/+} - E_{1/2}^{-/0}$ values, large CI guarantees orbital contributions from multiple high-lying filled and low-lying empty levels for **PZn-Sp-PZn** electronically excited states. Such CI ensures that the low-lying singlet of these species will possess both global delocalization and extensive quinoidal character (vide infra).

Transient Optical Spectra of PZn-Sp-PZn Initially Prepared Electronically Excited Singlet States. The combination of steady-state electronic absorption, potentiometric, and computational data, coupled with the expectation that substantial CI drives global electronic delocalization in electronically excited **PZn-Sp-PZn** species, suggests that quinoidal resonance contributions to S_1-S_n states exceed that for the corresponding ground (S_0) states. Pump−probe transient absorption spectroscopic experiments that interrogate the $S_1 \rightarrow S_n$ transition manifolds of these supermolecules further support this view. Figure 10 shows transient absorption spectra recorded at 300 fs time delay for **PZnE-EPZn, PZnE-BTD-EPZn, PZnE-PC-EPZn**, **PZnE-TDQ-EPZn**, and **PZnE-BBTD-EPZn** in the NIR spectral region.

Qualitatively, these $S_1 \rightarrow S_n$ spectra bear many features in common with those previously delineated for meso-to-meso ethyne-bridged bis[(porphinato)zinc(II)] (**PZn-E-PZn**) structures.[22] Like **PZn-E-PZn** species**, PZn-Sp-PZn** supermolecules display *intense* NIR $S_1 \rightarrow S_n$ transitions; these absorptions possess integrated oscillator strengths of comparable magnitude to their corresponding B- and Q-state manifold bleaching transitions (data not shown). While the benchmark **PZnE-EPZn** transient absorption spectrum (Figure 10A) bears features closely

(68) Salzner, U. *J. Phys. Chem. B* **2002**, *106*, 9214−9220.

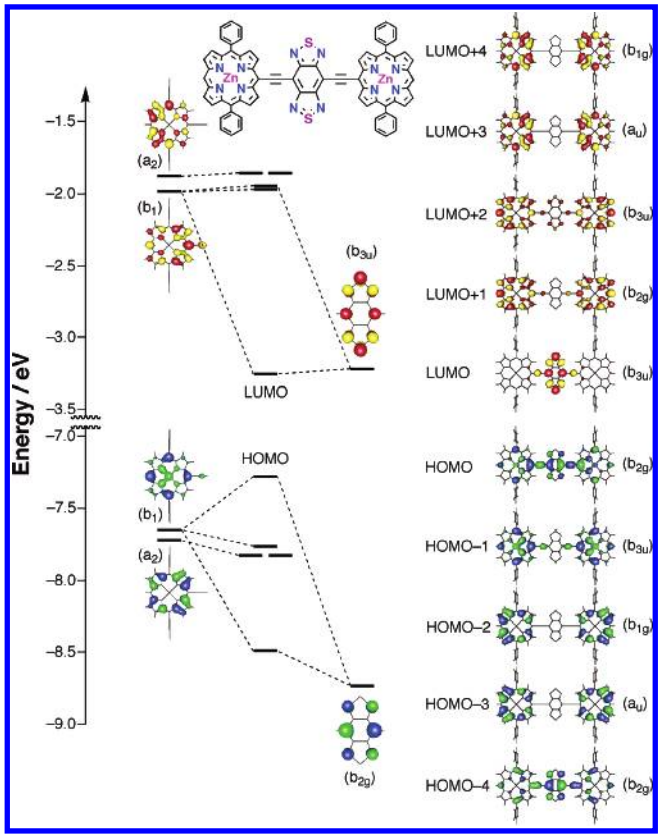

Figure 8. Frontier orbital correlation diagram for **PZnE**, benzobis(thiadiazole) (**BBTD**), and **PZnE-BBTD-EPZn**.

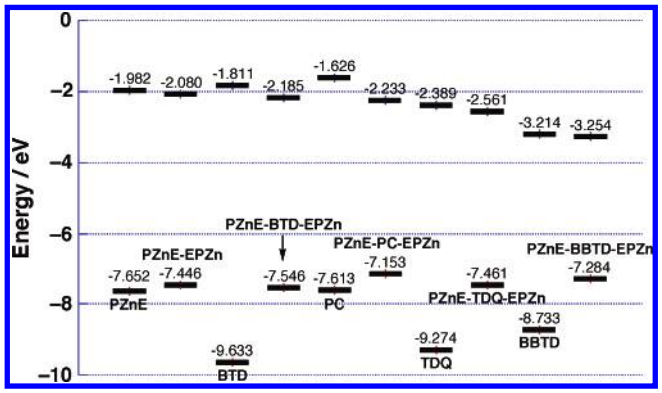

Figure 9. Diagrammatic representation of **PZn-Sp-PZn** and Sp HOMO and LUMO energy levels calculated using the PM3 semiempirical method.

aligned with that reported for **PZn-E-PZn** chromophores (bis-[(5,5′-10,20-bis[3,5-bis(3,3-dimethyl-1-butyloxy)phenyl]porphinato)zinc(II)]ethyne and [(5,-10,20-bis[3,5-bis(3,3-dimethyl-1-butyloxy)phenyl]porphinato)zinc(II)]-[(5′,-15′-ethynyl-10′,20′-bis(heptafluoropropyl)porphinato)zinc(II)]ethyne),[22] **PZnE-BTD-EPZn, PZnE-PC-EPZn**, **PZnE-TDQ-EPZn**, and **PZnE-BBTD-EPZn** manifest $S_1 \rightarrow S_n$ absorption manifolds that shift to progressively lower energies (Figure 10B−E), tracking with expectations based on the relative frontier orbital energy levels of these supermolecules determined by potentiometric and computational methods (vide supra).

The wavelength of the most intense transition within the NIR absorption manifold [$\lambda_{max}(S_1 \rightarrow S_n)$] for **PZnE-BTD-EPZn, PZnE-PC-EPZn**, **PZnE-TDQ-EPZn**, and **PZnE-BBTD-EPZn** occurs at 1207, ∼1187, 1270, and 1610 nm, respectively, 1700−3800 cm^{-1} red-shifted from the analogous $\lambda_{max}(S_1 \rightarrow S_n)$

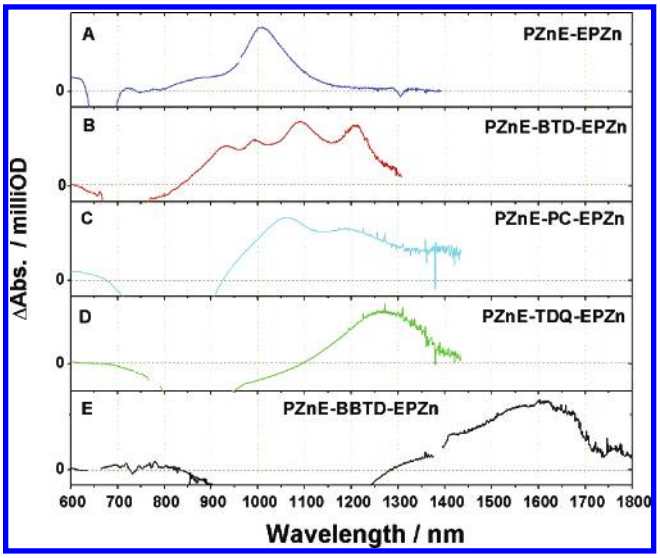

Figure 10. Scaled magic angle transient absorption spectra recorded for: (A) **PZnE-EPZn**, (B) **PZnE-BTD-EPZn**, (C) **PZnE-PC-EPZn**, (D) **PZnE-TDQ-EPZn**, and (E) **PZnE-BBTD-EPZn** measured at a delay time of 300 fs. Experimental conditions: solvent = THF; T = 25 °C; λ_{ex} = 655 nm (A), 662 nm (B), 775 nm (C), 775 nm (D), and 650 nm (E).

determined for **PZnE-EPZn** (∼1000 nm). Note that the corresponding fwhm values for the $S_1 \rightarrow S_n$ manifolds of these **PZn−Sp-PZn** species [Compound, (fwhm): **PZnE-BTD-EPZn** (∼2800 cm^{-1}), **PZnE-PC-EPZn** (>2500 cm^{-1}), **PZnE-TDQ-EPZn** (≥1160 cm^{-1}) and **PZnE-BBTD-EPZn** (≥1150 cm^{-1})] determined at 300 fs following optical excitation, meet or exceed that evinced for **PZnE-EPZn** (1100 cm^{-1}).

Further, the Figure 10B−E spectra bear absorptive signatures that indicate that the nature of the proquinoidal bridge plays a pivotal role in determining the degree of excited-state conjugation and the extent to which nuclear relaxation dynamics[69] impact the early-time evolution of the excited state. As a case in point, note that while sharp differences exist between the $S_0 \rightarrow S_1$ absorption manifolds of **PZnE-BTD-EPZn** and **PZnE-PC-EPZn** (Figure 2), the low energy excited states for these species present 300 fs following optical excitation are similar, with significant NIR-absorptive spectral breadths and substantial $S_1 \rightarrow S_n$ absorptive oscillator strengths at wavelengths longer than 1300 nm. In this regard, we underscore that there are relatively few examples of electronically excited chromophoric singlet states that absorb strongly in the NIR; systems that exhibit such singlet excited-state manifold absorptive properties are largely confined to a select group of semiconducting π-conjugated polymers.[70−76]

Conclusion

Conjugated (porphinato)zinc(II)-spacer-(porphinato)zinc(II) (**PZn-Sp-PZn**) complexes that possess intervening conjugated

(69) Duncan, T. V.; Susumu, K.; Therien, M. J., manuscript in preparation.
(70) Moraes, F.; Schaffer, H.; Kobayashi, M.; Heeger, A. J.; Wudl, F. *Phys. Rev. B* **1984**, *30*, 2948−2950.
(71) Woo, H. S.; Graham, S. C.; Halliday, D. A.; Bradley, D. D. C.; Friend, R. H.; Burn, P. L.; Holmes, A. B. *Phys. Rev. B* **1992**, *46*, 7379−7389.
(72) Lanzani, G.; Nisoli, M.; De Silvestri, S.; Barbarella, G.; Zambianchi, M.; Tubino, R. *Phys. Rev. B* **1996**, *53*, 4453−4457.
(73) Frolov, S. V.; Liess, M.; Lane, P. A.; Gellermann, W.; Vardeny, Z. V.; Ozaki, M.; Yoshino, K. *Phys. Rev. Lett.* **1997**, *78*, 4285−4288.
(74) Kraabel, B.; Klimov, V. I.; Kohlman, R.; Xu, S.; Wang, H.-L.; McBranch, D. W. *Phys. Rev. B* **2000**, *61*, 8501−8515.
(75) Kraabel, B.; McBranch, D. W. *Chem. Phys. Lett.* **2000**, *330*, 403−409.
(76) Jiang, X. M.; Österbacka, R.; Korovyanko, O.; An, C. P.; Horovitz, B.; Janssen, R. A. J.; Vardeny, Z. V. *Adv. Funct. Mater.* **2002**, *12*, 587−597.

Sp structures with varying degrees of proquinoidal character have been synthesized by palladium-catalyzed cross coupling reactions. These supermolecular **PZn-Sp-PZn** compounds feature Sp moieties {(4,7-diethynylbenzo[*c*][1,2,5]thiadiazole (**E-BTD-E**), 6,13-diethynylpentacene (**E-PC-E**), 4,9-diethynyl-6,7-dimethyl[1,2,5]thiadiazolo[3,4-*g*]quinoxaline (**E-TDQ-E**), and 4,8-diethynylbenzo[1,2-*c*:4,5-*c*′]bis([1,2,5]thiadiazole) (**E-BBTD-E**)} that regulate frontier orbital energy levels and progressively increase the extent of the quinoidal resonance contribution to the ground and electronically excited states, augmenting the magnitude of electronic communication between terminal (5,-10,20-di(aryl)porphinato)zinc(II) units, relative to that evinced for a bis[(5,5′,-10,20-di(aryl)porphinato)zinc(II)]-butadiyne benchmark (**PZnE-EPZn**). Electronic absorption spectra show significant red-shifts of the respective **PZn-Sp-PZn** x-polarized Q state ($S_0 \rightarrow S_1$) transition manifold maxima (240−4810 cm^{-1}) relative to that observed for **PZnE-EPZn**. Likewise, the potentiometrically determined **PZn-Sp-PZn** HOMO−LUMO gaps ($E_{1/2}^{0/+} - E_{1/2}^{-/0}$) display correspondingly diminished energy separations that range from 1.88 to 1.11 eV relative to that determined for **PZnE-EPZn** (2.01 eV). Electronic structure calculations show that while all **PZn-Sp-PZn** structures possess delocalized HOMOs, structures having benzothiadiazole- and pentacene-based spacers exhibit delocalized LUMOs, while analogous compounds based on thiadiazoloquinoxaline and benzobis(thiadiazole)-derived bridging moieties evince highly stabilized LUMO energy levels that feature Sp-localized electron density. Collectively, steady-state optical, potentiometric, and computational data point to the existence of **PZn-Sp-PZn** electronically excited singlet states that display augmented quinoidal character relative to the S_0 state.

Pump−probe transient spectral data for these **PZn-Sp-PZn** supermolecules are remarkable, and demonstrate that the $S_1 \rightarrow S_n$ transition manifolds of these species span an unusually broad spectral domain of the NIR. Notably, the absorption maxima of these $S_1 \rightarrow S_n$ manifolds can be tuned over a 1000−1600 nm spectral region, giving rise to intense excited-state transitions ∼4000 cm^{-1} lower in energy than that observed for the analogous excited-state absorption maximum of the **PZnE-EPZn** benchmark; these data highlight the unusually large quinoidal resonance contribution to the low-lying electronically excited singlet states of these **PZn-Sp-PZn** species. In this regard, we underscore that there are relatively few examples of electronically excited chromophoric singlet states that absorb strongly in the NIR; systems that possess such singlet excited-state manifold absorptive properties are largely confined to a select group of semiconducting π-conjugated polymers.[70−76] It is important to emphasize with respect to this comparison, however, that the classic intrachain $S_1 \rightarrow S_n$ absorption energies of highly conjugated phenylene- and thiophene-based polymers exceed 1 eV ($\lambda_{abs} < 1250$ nm).[70−76] The length scale spanned by the **PZn-Sp-PZn** structures (∼25 Å), and the fact that the NIR manifold absorptions chronicled in the Figure 10 data do not correspond to $T_1 \rightarrow T_n$ absorptions, or transitions related to the polaron absorption bands of semiconducting polymers[70−76] derived from charge-doping or intra- and interchain charge separated states, highlight the tremendous potential of these **PZn-Sp-PZn** species and their higher molecular weight analogues as electrooptic materials.

Acknowledgment. This work was supported through the National Cancer Institute (NO1-CO-29008), and the MRSEC Program of the National Science Foundation (DMR00-79909).

Supporting Information Available: Synthetic details, characterization data, synthetic schemes, details concerning ultrafast transient absorption experiments, electronic absorption spectra (**PZnE-TMS**, **BTD(E-TMS)$_2$**, **PC(E-TMS)$_2$**, **TDQ(E-TMS)$_2$**, and **BBTD(E-TMS)$_2$**), tabulated optical and electrochemical data, electronic structure computational data. This material is available free of charge via the Internet at http://pubs.acs.org.

JA040243H